RESEARCH ARTICLE

Check for updates

A chiral sodium lanthanum sulfate for second-order nonlinear optics and proton conduction†

Hao Fu,[a,b] Xiaohui Zhang,[a] Peiyu Liu,[a] Bo Li,[c] Baolin Wu,[d] Ye Tao,[a] Qianshuang Lu,[a] Yingjie Li,[a] Jiaxi Huang,[a] Fangfang Zhang, [ID][e] Tingchao He, [ID][f] Zhi Chen, [ID][a] Heng Wang,[g] Chenliang Su, [ID][b] Hong-Ying Zang,[c] Xiujun Yu [ID]*[a] and Xiaopeng Li [ID][a,g,h]

Chiral metal sulfates have demonstrated potential applications in various areas such as ferroelectricity and nonlinear optics (NLO) due to their non-centrosymmetric structural features. However, the synthesis of chiral metal sulfates remains a formidable challenge, as tuning the polarizability and anisotropy of the highly symmetric tetrahedral sulfate group is particularly difficult. In this context, we have rationally synthesized a chiral sodium lanthanum sulfate, $NaLa(SO_4)_2(H_2O)$, through the combination of alkali and rare-earth cations. The compound exhibits NLO response with a short absorption cutoff edge (<192 nm). Theoretical calculations suggest that the NLO response mainly originates from the synergistic cooperation of $[LaO_9]$ polyhedra and $[SO_4]$ tetrahedra. Furthermore, $NaLa(SO_4)_2(H_2O)$ may potentially achieve birefringence phase matching, as predicated by high birefringence (0.13 @ 1064 nm) in theoretical calculations. Additionally, $NaLa(SO_4)_2(H_2O)$ shows a high proton conductivity of 3.22×10^{-3} S cm^{-1} under 85 °C and 98% relative humidity. The complementary cation strategy of this work offers a new paradigm for the controllable synthesis of chiral metal sulfates and development of functional materials.

Introduction

Metal sulfates have broad applications in optics, magnetism, catalysis and proton conduction due to their diverse structures, which arise from the abundant coordination modes between sulfate ($[SO_4]$) tetrahedra and metal cations.[1–9] Chiral

[a]College of Chemistry and Environmental Engineering, Shenzhen University, Shenzhen, Guangdong 518060, China. E-mail: xiujunyu@szu.edu.cn
[b]Institute of Microscale Optoelectronics, Shenzhen University, Shenzhen, Guangdong 518060, China
[c]Key Laboratory of Polyoxometalate Science, Department of Chemistry, Northeast Normal University, Changchun, Jilin 130024, China
[d]Fundamental electrochemistry (IET-1), Institute of Energy Technologies, Forschungszentrum Jülich GmbH, Wilhelm-Johnen-Straße, Jülich 52425, Germany
[e]Research Center for Crystal Materials, Xinjiang Technical Institute of Physics and Chemistry, Chinese Academy of Sciences, Urumqi, Xinjiang 830011, China
[f]Key Laboratory of Optoelectronic Devices and Systems of Ministry of Education and Guangdong Province, College of Physics and Optoelectronic Engineering, Shenzhen University, Shenzhen, Guangdong 518060, China
[g]State Key Laboratory of Organometallic Chemistry, Shanghai Institute of Organic Chemistry, University of Chinese Academy of Sciences, Chinese Academy of Sciences, Shanghai 200032, China
[h]Shenzhen University General Hospital, Shenzhen University Clinical Medical Academy, Shenzhen University, Shenzhen, Guangdong 518055, China
† Electronic supplementary information (ESI) available. CCDC 2351005. For ESI and crystallographic data in CIF or other electronic format see DOI: https://doi.org/10.1039/d4qi01708k

metal sulfates, in particular, have garnered significant attention for their potential applications in ferroelectricity and nonlinear optics (NLO) owing to their non-centrosymmetric structural features.[10–16] For instance, as non-π-conjugated clusters, the aligned anionic $[SO_4]$ groups often exhibit a notable second harmonic generation (SHG) response and a wide transmittance window, making them potential candidates for deep ultraviolet (UV) second-order NLO crystals.[11–16] However, the synthesis of chiral metal sulfates remains a formidable challenge, as tuning the polarizability and anisotropy of the highly symmetric tetrahedral $[SO_4]$ group is particularly difficult.

To obtain chiral metal sulfates, the introduction of diverse metal cations with local asymmetric units is an efficient strategy to generate macroscopic asymmetry.[17–25] These cations can be classified into: (1) d^{10} cations with a vulnerable displacement, *e.g.*; Zn^{2+}, Cd^{2+};[11,17,18] (2) d^0 electronic configuration cations with distorted octahedral coordination, for example, W^{6+} and Ti^{4+};[19,20] (3) cations with stereochemically active lone pairs, *e.g.*; Sn^{2+}, Pb^{2+}, and Bi^{3+};[11,19,21,22] (4) alkali/alkaline-earth cations with no d–d electron or f–f electron transitions in UV region;[11–16,19,23–25] (5) rare-earth cations containing distortive polyhedra with relatively large hyperpolarizability.[26] It is worth noting that rare-earth cations, especially Sc^{3+}, Y^{3+}, La^{3+}, Gd^{3+}, and Lu^{3+}, which lack unclosed d or f electrons, may effectively avoid unfavorable d–d or f–f electronic transitions and have recently been employed to prepare NLO-active chiral

metal sulfates.[26] Additionally, rare-earth cations exhibit intriguing topologies and coordination modes due to the accessibility of higher coordination numbers. However, incorporating two or more synergistic cations into chiral sulfates represents a substantial challenge attributed to the difficulty in rationally assembling local asymmetric units.

In this context, through the complementary integration of alkali and rare-earth cations, we have rationally synthesized a chiral sodium lanthanum sulfate, $NaLa(SO_4)_2(H_2O)$ (Scheme 1a). The compound exhibits SHG response with a short absorption cutoff edge (<192 nm, Scheme 1b). Theoretical calculations suggest that the synergistic cooperation of $[LaO_9]$ polyhedra and $[SO_4]$ tetrahedra mainly contributes to the SHG response and high birefringence, potentially achieving birefringence phase matching. Furthermore, $NaLa(SO_4)_2(H_2O)$ shows a high proton conductivity of 3.22×10^{-3} S cm^{-1} under 85 °C and 98% relative humidity (Scheme 1c). Notably, since such complementary cation strategy may be applied to other alkali/alkaline-earth cations and rare-earth cations, this work can pave a new avenue for the controllable synthesis of functional chiral metal sulfates.

Results and discussion

The compound $NaLa(SO_4)_2(H_2O)$ was synthesized through a complementary strategy involving the combination of Na^+ and La^{3+}. This approach demonstrates robustness across a wide range of temperatures (120–200 °C), concentrations, and pH levels (see details in the ESI†). Single-crystal X-ray diffraction (SCXRD) analysis revealed that $NaLa(SO_4)_2(H_2O)$ crystallizes in the chiral trigonal space group $P3_221$ (No. 154) with unit cell parameters of $a = 7.060(4)$ Å, $b = 7.060(4)$ Å, and $c = 12.953(8)$ Å. The chiral $NaLa(SO_4)_2(H_2O)$ exhibits an overall sma-type topology (Fig. 1a, b and S1†). The coordination numbers of La^{3+} and Na^+ are 9 and 8, respectively (Fig. 1b). Each La atom is coordinated to eight oxygen atoms from six $[SO_4]$ tetrahedra (four of them contributing one oxygen atom and two of them providing two), and one oxygen atom from a water molecule.
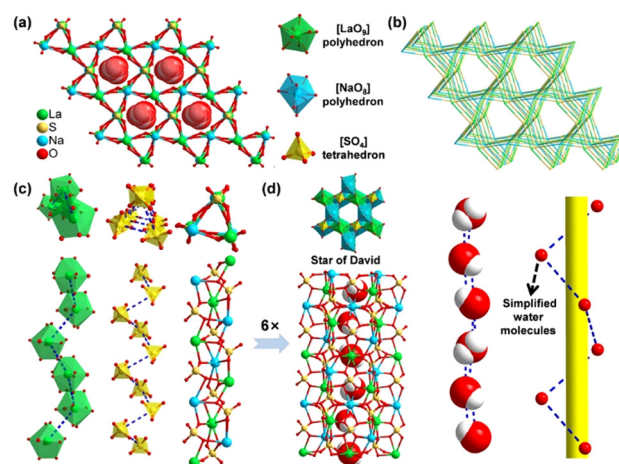
Fig. 1 Crystal structure of $NaLa(SO_4)_2(H_2O)$. (a) Simplified sma topology. (b) View of the framework along the c axis. (c) 1D triangular prism $[NaLa(SO_4)_2]_\infty$ (right), and packing manners of $[LaO_9]$ polyhedron (left) and $[SO_4]$ tetrahedron (middle). (d) Structure of 1D pore (nanotube, left) and spiral water chain in the nanotube (right).

Each Na atom is similarly coordinated to eight oxygen atoms from six $[SO_4]$ groups. The Na atoms and La atoms are linked by $[SO_4]$ tetrahedra to form an infinite chiral triangular prism 1D-hain, $[NaLa(SO_4)_2]_\infty$ (Fig. 1c and S2†). In this triangular prism, the La, Na and S atoms form a spiral chain with an ordered arrangement of –La–S–Na–S–. Each 1D-triangular prism is connected to three adjacent prisms by sharing Na and La atoms, further assembling into a sma-type framework with $[SO_4]$ units acting as 4-connected nodes (Fig. 1b). The $[LaO_9]$ polyhedron and $[SO_4]$ tetrahedron are uniformly arranged along the c-axis in a spiral pattern (Fig. 1c), and such spiral arrangement is beneficial for enhancing SHG effect due to the increased microscopic second-order susceptibility.

Interestingly, a chiral nanotube is formed by linking six 1D-triangular prisms of $[NaLa(SO_4)_2]_\infty$ (Fig. 1d). A top view along the c-direction of this chiral nanotube resembles the "Star of David" (Fig. 1d). A careful examination of the simplified topology (with sulfate units omitted) of $\{Na_3La_3\}$ hexagonal rings
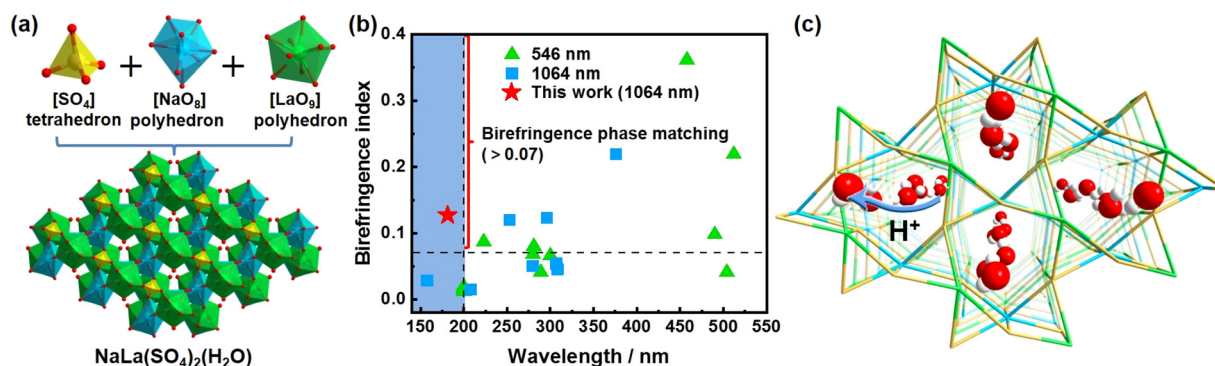
Scheme 1 (a) Synthesis of $NaLa(SO_4)_2(H_2O)$ using a complementary cation strategy. (b) Comparison of birefringence with the literature.[11,18,21–35] (c) 1D spiral water chain promoted high proton conductivity of $NaLa(SO_4)_2(H_2O)$.

This journal is © the Partner Organisations 2024

Inorg. Chem. Front., 2024, **11**, 7026–7033 | **7027**

on the surface of this nanotube is reminiscent of the {C$_6$} hexagons in carbon nanotubes (Fig. S3†). Furthermore, in each chiral nanotube, two chains of –La–S–Na–S– form a double helical structure similar to DNA on the inner wall of the nanotube. The [LaO$_9$] polyhedron and [SO$_4$] tetrahedron are also arranged in a double-helical manner around the nanowall (Fig. S4†). Surprisingly, the interior 1D pore of the framework is filled with nanoconfined water molecules, which form a water helix corresponding to the 3$_2$ axis through hydrogen bonding (Fig. 1d). These water molecules are weakly co-ordinated with La atoms on the inner wall of the nanotube and are stacked one by one in a 120° staggered manner in the center of the 1D pore, forming spiral nanowires as observed from the single-crystal structure (Fig. 1d). The polar water helices may enhance nonlinear optical susceptibilities. In addition, the spirally aligned water molecules could contribute to high proton conductivity by serving as a potential proton transport channel. Detailed studies on SHG response and proton conductivity are described in the following sections.

The compound of NaLa(SO$_4$)$_2$(H$_2$O) is further fully characterized by various spectroscopic methods. The phase purity of the polycrystalline sample was confirmed by the powder X-ray diffraction (PXRD) analysis as the experimental PXRD pattern of NaLa(SO$_4$)$_2$(H$_2$O) corresponds closely with the simulated pattern based on the crystallographic data (Fig. 2a). Thermogravimetric analyses of NaLa(SO$_4$)$_2$(H$_2$O) were further performed under a nitrogen atmosphere. As shown in Fig. 2b, the weight loss of 4.8% at the temperature range of 180–400 °C corresponds to the release of water molecules in 1D pore (theoretical loss of 4.7%). The infrared (IR) spectrum of the crystalline NaLa(SO$_4$)$_2$(H$_2$O) revealed the existence of [NaO$_8$],

[LaO$_9$] and [SO$_4$] structural building units (Fig. 2c). Specifically, the IR band at the range of 3638–3430 cm^{-1} confirms the presence of water molecules. The peak at 1617 cm^{-1} can be assigned to the bending vibrations of coordination water. The broad peak at 1100 cm^{-1} can be attributed to the stretching vibrations of [SO$_4$] groups and their bending vibrations appear at around 660 cm^{-1}. Moreover, the peaks at 487 cm^{-1} and range of 555–705 cm^{-1} belong to the vibrations of the [NaO$_8$] and [LaO$_9$] polyhedra, respectively. The UV/visible-near-infrared (UV/Vis-NIR) diffuse reflectance spectrum and its transformed absorption spectrum of NaLa(SO$_4$)$_2$(H$_2$O) reveal a UV absorption edge clearly below 192 nm, with the reflectance *ca.* 69% at 192 nm, indicating that NaLa(SO$_4$)$_2$(H$_2$O) possesses a short wavelength deep-UV absorption edge (Fig. 2d and S6†). The bandgap of NaLa(SO$_4$)$_2$(H$_2$O) is comparable to reported deep-UV NLO alkali metal/alkaline-earth metal-based sulfates, such as Li$_9$Na$_3$Rb$_2$(SO$_4$)$_7$ [12] and Cs$_2$BeS$_2$(SO$_4$)$_2$.[23] Notably, the compound NaLa(SO$_4$)$_2$(H$_2$O) exhibits excellent stability under high humidity and temperature conditions (Fig. S7†), making it highly suitable for practical applications.

The second-order NLO properties of NaLa(SO$_4$)$_2$(H$_2$O) were evaluated on a home-built femtosecond laser pumped single crystal NLO measurement setup (Fig. S8†).[36] As shown in Fig. 3a, power-dependent SHG response of a NaLa(SO$_4$)$_2$(H$_2$O) microcrystal pumped at 860 nm confirm the second-order NLO activity of the chiral sodium lanthanum sulfate. Moreover, wavelength-dependent NLO spectra exhibit clear second harmonic peaks when pumped at various wavelengths over the near-infrared region of 780–920 nm (Fig. S9†). The effective second-order NLO coefficient (d_{eff}) of NaLa(SO$_4$)$_2$(H$_2$O) is esti-
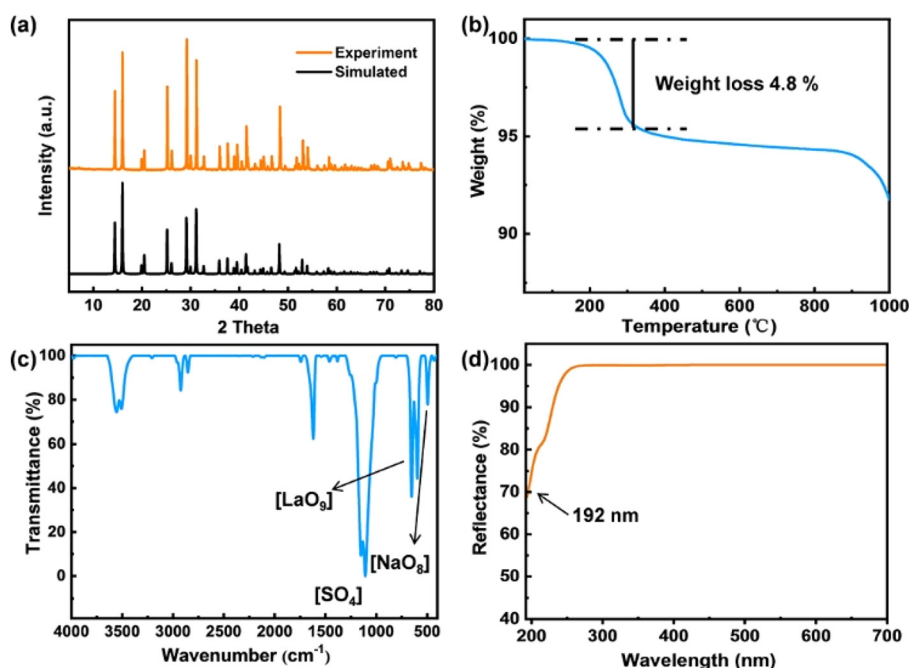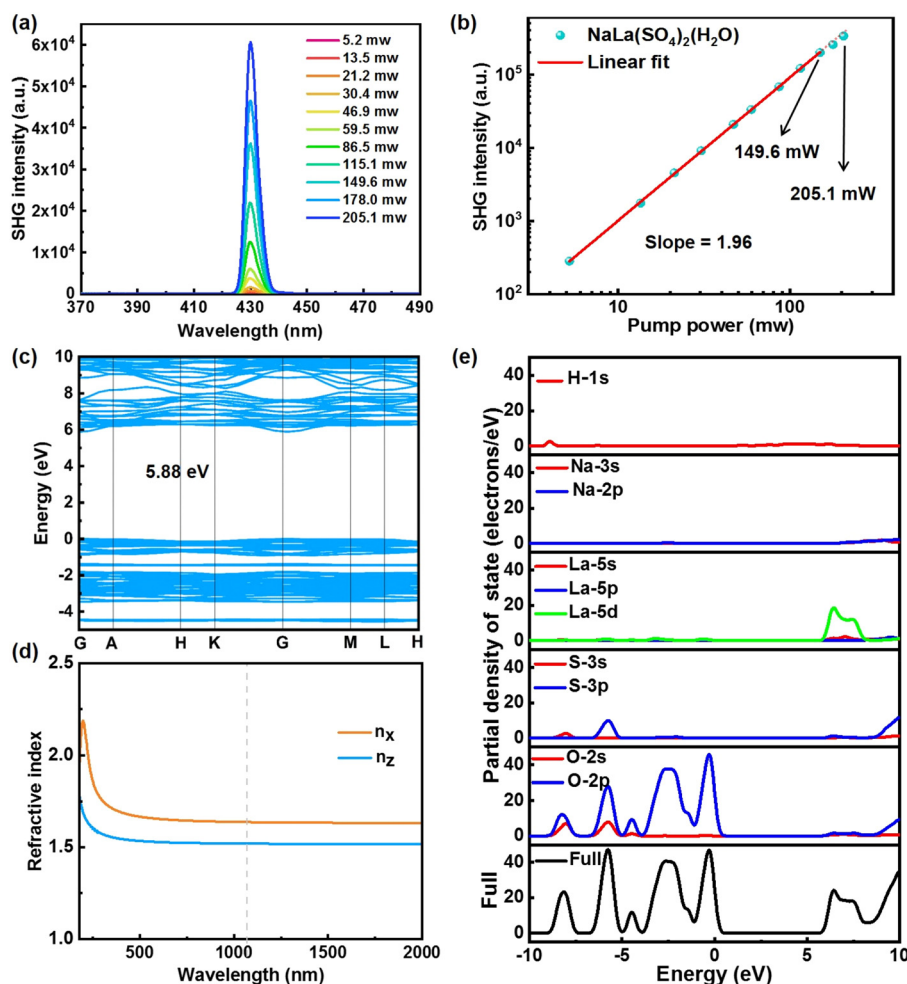

Fig. 2 PXRD pattern (a), thermogravimetric analyses (b), IR spectrum (c) and UV/Vis-NIR spectrum (d) of NaLa(SO$_4$)$_2$(H$_2$O).

Fig. 3 (a) SHG spectra pumped at various excitation power at 860 nm. (b) Logarithmic plot of SHG intensity as function of the incident power, pumped at 860 nm (to avoid the issue of signals exceeding the detection range). (c) Electronic band structure of $NaLa(SO_4)_2(H_2O)$. (d) Calculated dispersion of refractive index curves of $NaLa(SO_4)_2(H_2O)$. (e)Total and partial density of states of $NaLa(SO_4)_2(H_2O)$.

mated to be ~0.21 pm V^{-1} with the optimized linearly polarized pump at 860 nm by using a Y-cut quartz as the reference, suggesting a moderate SHG efficiency.[37] Additionally, the SHG intensity shows a quadratic dependence on the incident laser power, verifying the two-photon nature of this second-order NLO response (Fig. 3b). Notably, the SHG intensity remains the same within 2 minutes when the laser power is maintained as high as ~150 mW (860 nm), suggesting the high laser damage threshold of $NaLa(SO_4)_2(H_2O)$ (Fig. 3b and S10†). Unfortunately, we could not obtain the laser damage threshold of $NaLa(SO_4)_2(H_2O)$ since the expected powder is out of the limit of our setup. Polarization-dependent SHG intensity demonstrates a quadrupolar profile (Fig. S11†), and the polarization ratio is calculated as 0.19.

To deeply understand the origin of SHG response, electronic structures and birefringence phase-matchable performance are further investigated by the density functional theory (DFT) methods.[38] The electronic band structure calculation suggests that the direct band gap of $NaLa(SO_4)_2(H_2O)$ is 5.88

eV (Fig. 3c), which is smaller than the experimental value (>6.2 eV), since the energy bandgap is usually underestimated when adopting the generalized gradient approximation (GGA) method with the Perdew–Burke–Ernzerhof (PBE) function due to the limitation of DFT calculation.[23] The refractive index dispersion curves of $NaLa(SO_4)_2(H_2O)$ are also lucubrated and the birefringence is estimated as 0.13 at 1064 nm (Fig. 3d), indicating the phase-matching ability of $NaLa(SO_4)_2(H_2O)$ in the deep-UV NLO process. Furthermore, electron transition between states near the Fermi level and structural distortion of coordination polyhedra could mainly contribute to the SHG response. As such, partial density of states projected onto specific atoms are calculated and presented in Fig. 3e. The highest valence band (VB) is determined by the O 2p nonbonding orbitals, whereas the empty O 2p, La 6d, and S 3p states majorly contribute to the lowest conduction band (CB). The orbitals of blue-shift cation (Na^+ in our case) exhibit no obvious contribution to the bandgap. Therefore, the orbitals of [SO_4] and [LaO_9] units define the highest VB and lowest CB.

This journal is © the Partner Organisations 2024

Inorg. Chem. Front., 2024, **11**, 7026–7033 | **7029**

Consequently, the $[LaO_9]$ polyhedral (especially the two short La–O bonds, La01–O004 and La01–O004,[4] Fig. S5†) and $[SO_4]$ tetrahedra have significant contributions to the density of states near the forbidden band and thus play a key role in determining the second-order nonlinear optical performance.

Considering the existence of sulfate tetrahedra as proton hopping sites and water-derived hydrogen-bonded chain, the $NaLa(SO_4)_2(H_2O)$ could be a good candidate of proton conductor. To assess its proton conducting performance, alternating current impedance spectroscopy measurements using compacted pellets of the crystalline powder were conducted under 70–98% relative humidity at 30 °C. The impedance spectra of the compound are shown in Fig. 4a and their bulk and total proton conductivities were determined from the semicircles in the Nyquist plots. The semicircle in the high-frequency region relates to the bulk and grain boundary resistances, and the tail in the low-frequency region corresponds to the mobile ions, which are blocked by the interface between electrode and electrolyte.[39] Such results reveal that the bulk proton conductivity of $NaLa(SO_4)_2(H_2O)$ increases rapidly with the increase of humidity and reaches 5.77×10^{-6} S cm^{-1} at 30 °C and 98% relative humidity. To verify the humidity dependent proton conducting property of $NaLa(SO_4)_2(H_2O)$, water vapor absorption and desorption isotherms were measured at 298 K. As shown in Fig. 4b, the water vapor adsorption of $NaLa(SO_4)_2(H_2O)$ increases with the increasing humidity, which is consistent with the change of proton conductivity, suggesting

that the compound is humidity dependent proton conductor. Besides, under high humidity, the highest water vapor uptake of $NaLa(SO_4)_2(H_2O)$ can reach 151.3 mg g^{-1}, suggesting that the compound is highly hydrophilic, probably due to the existence of abundant sulfate groups that can easily form strong hydrogen bonds with adsorbed water molecules. The proton conductivity of $NaLa(SO_4)_2(H_2O)$ was further investigated at 30–85 °C under a constant relative humidity of 98%. As depicted in Fig. 4c, with the temperature increase from 30 to 85 °C, the bulk conductivity of $NaLa(SO_4)_2(H_2O)$ increase obviously from 5.77×10^{-6} to 3.22×10^{-3} S cm^{-1}, showing typical temperature dependent proton conductivity. To gain insight into their proton transfer mechanism, the activation energy (E_a) of $NaLa(SO_4)_2(H_2O)$ at 98% relative humidity and 30–85 °C was calculated according to the Arrhenius equation (Fig. 4d). The result reveals that $NaLa(SO_4)_2(H_2O)$ shows an E_a of 0.96 eV, suggesting that the dominated proton conduction mechanism for this compound is vehicle mechanism (accomplishes proton transport by diffusive routes, generally with $E_a > 0.4$ eV).[40] Therefore, we conclude that the high photon conducting performance of $NaLa(SO_4)_2(H_2O)$ can be attributed to the multiple sulfate groups in the structure that can not only act as proton hopping sites but also easily form extensive hydrogen-bonded chains with adsorbed water molecules for promoting proton transport.[39–43] In addition, 1D spiral chain of water molecules formed through hydrogen bonding facilitates proton conduction. It is worth noting that the high
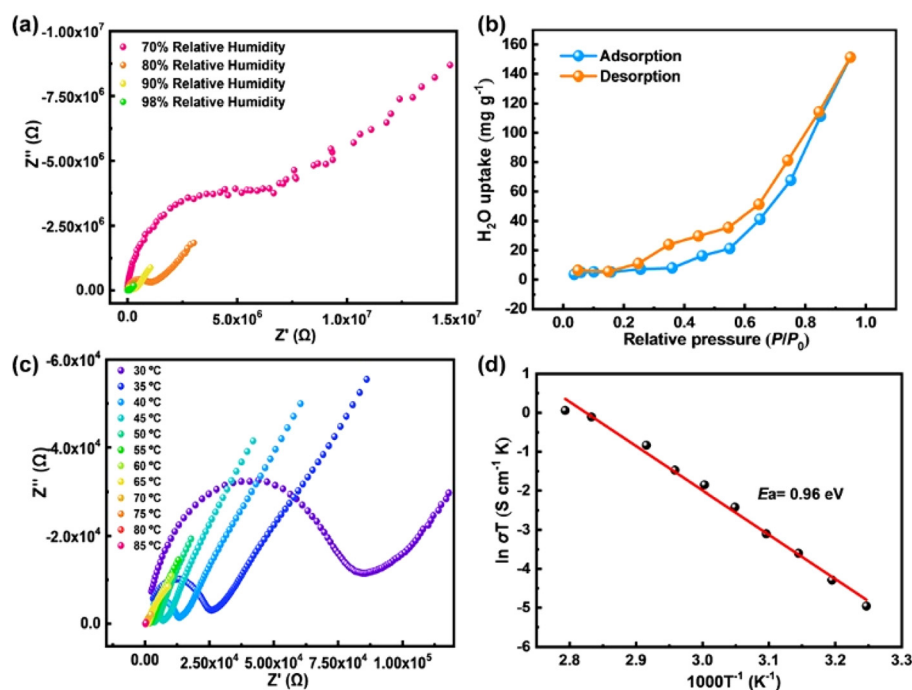
Fig. 4 (a) Nyquist plots of $NaLa(SO_4)_2(H_2O)$ at 30 °C and various humidity variations from 70% to 98%. (b) Water vapor adsorption and desorption isotherms of $NaLa(SO_4)_2(H_2O)$ at 298 K. (c) Nyquist plots of $NaLa(SO_4)_2(H_2O)$ at 98% relative humidity and various temperature variations from 30 to 85 °C. (d) Arrhenius plot of $NaLa(SO_4)_2(H_2O)$ under 98% relative humidity and different temperature variations from 30 to 85 °C.

proton conductivity of $NaLa(SO_4)_2(H_2O)$ is among the highest values reported for sulfate-based compounds.[41–43]

Conclusions

In summary, we have successfully synthesized a chiral sodium lanthanum sulfate, namely $NaLa(SO_4)_2(H_2O)$, through the complementary integration of alkali and rare-earth cations. The compound exhibits SHG response with a short absorption cutoff edge (<192 nm), and a high birefringence (0.13@1064 nm, estimated by theoretical calculations), indicating that $NaLa(SO_4)_2(H_2O)$ could become a potential deep-UV transparent NLO material. Detailed theoretical calculations suggest that the NLO performance mainly originates from the synergistic cooperation of $[LaO_9]$ polyhedra and $[SO_4]$ tetrahedra. Notably, $NaLa(SO_4)_2(H_2O)$ shows a high proton conductivity of 3.22×10^{-3} S cm^{-1} under 85 °C and 98% relative humidity. Our study provides a new paradigm for the controllable synthesis of chiral metal sulfates and the development of functional materials, enabling a deeper understanding of the structure–property relationship. Importantly, the complementary cation strategy described in this work can be further applied to other alkali/alkaline-earth cations and rare-earth cations. Work along this line is currently ongoing in our laboratory.

Author contributions

X. Y. conceived and coordinated all stages of this research. H. F., X. Z., P. L., Q. L., Y. L. and J. H. carried out the synthesis and characterization of the compound. Y. T., T. H. and F. Z. studied the second-order nonlinear optical properties. B. L. and H.-Y. Z. provided the measurements of proton conductivity. B. W. performed the theoretical calculations. Z. C., H. W., C. S. and X. L. assisted with data analysis. All the authors were actively involved in development of the manuscript.

Data availability

The data that support the findings of this study are available in the ESI† of this article.

Conflicts of interest

There are no conflicts to declare.

Acknowledgements

References

1 M. S. Wickleder, Inorganic lanthanide compounds with complex anions, *Chem. Rev.*, 2002, **102**, 2011–2087.

2 C. Cui, W. Ju, X. Luo, Q. Lin, J. Cao and Y. Xu, A series of lanthanide compounds constructed from Ln_8 rings exhibiting large magnetocaloric effect and interesting luminescence, *Inorg. Chem.*, 2018, **57**, 8608–8614.

3 B. Yotnoi, A. Rujiwatra, M. L. P. Reddy, D. Sarma and S. Natarajan, Lanthanide sulfate frameworks: synthesis, structure, and optical properties, *Cryst. Growth Des.*, 2011, **11**, 1347–1356.

4 R. F. D'Vries, M. Iglesias, N. Snejko, S. Alvarez-Garcia, E. Gutiérrez-Puebla and M. A. Monge, Mixed lanthanide succinate-sulfate 3D MOFs: Catalysts in nitroaromatic reduction reactions and emitting materials, *J. Mater. Chem.*, 2012, **22**, 1191–1198.

5 L.-Y. Xu, J.-P. Zhao, T. Liu and F.-C. Liu, Gadolinium sulfate modified by formate to obtain optimized magneto-caloric effect, *Inorg. Chem.*, 2015, **54**, 5249–5256.

6 S.-D. Han, X.-H. Miao, S.-J. Liu and X.-H. Bu, Magnetocaloric effect and slow magnetic relaxation in two dense (3,12)-connected lanthanide complexes, *Inorg. Chem. Front.*, 2014, **1**, 549–552.

7 L. Liu, H. Meng, G. Li, Y. Cui, X. Wang and W. Pang, $[C_2N_2H_{10}]_{1.5}[Nd(SO_4)_3(H_2O)]\cdot 2H_2O$: The first organically templated neodymium sulfate with a layer structure, *J. Solid State Chem.*, 2005, **178**, 1003–1007.

8 H. Yang, C. Xu, Z. Li, M. Li and G. Liu, Synthesis, characterization and optical properties of three novel lanthanide sulfates, *J. Solid State Chem.*, 2021, **303**, 122481.

9 J. Perles, C. Fortes-Revilla, E. Gutiérrez-Puebla, M. Iglesias, M. Á. Monge, C. Ruiz-Valero and N. Snejko, Synthesis, structure, and catalytic properties of rare-earth ternary sulfates, *Chem. Mater.*, 2005, **17**, 2701–2706.

10 H. Fan, N. Ye and M. Luo, New functional groups design toward high performance ultraviolet nonlinear optical materials, *Acc. Chem. Res.*, 2023, **56**, 3099–3109.

11 Y. Shang, J. Xu, H. Sha, Z. Wang, C. He, R. Su, X. Yang and X. Long, Nonlinear optical inorganic sulfates: The improvement of the phase matching ability driven by the structural modulation, *Coord. Chem. Rev.*, 2023, **494**, 215345.

12 Y. Li, F. Liang, S. Zhao, L. Li, Z. Wu, Q. Ding, S. Liu, Z. Lin, M. Hong and J. Luo, Two non-π-conjugated deep-UV nonlinear optical sulfates, *J. Am. Chem. Soc.*, 2019, **141**, 3833–3837.

13 Y. Li, S. Zhao, P. Shan, X. Li, Q. Ding, S. Liu, Z. Wu, S. Wang, L. Li and J. Luo, $Li_8NaRb_3(SO_4)_6\cdot 2H_2O$ as a new

This journal is © the Partner Organisations 2024

Inorg. Chem. Front., 2024, **11**, 7026–7033 | **7031**

sulfate deep-ultraviolet nonlinear optical material, *J. Mater. Chem. C*, 2018, **6**, 12240–12244.

14 Y. Li, C. Yin, X. Yang, X. Kuang, J. Chen, L. He, Q. Ding, S. Zhao, M. Hong and J. Luo, A nonlinear optical switchable sulfate of ultrawide bandgap, *CCS Chem.*, 2020, **3**, 2298–2306.

15 H. Sha, J. Xu, Z. Xiong, Z. Wang, R. Su, C. He, X. Yang, X. Long and Y. Liu, An optimized $KBe_2BO_3F_2$–like structure: The unity of deep–ultraviolet transparency, nonlinear optical property, and ferroelectricity, *Adv. Opt. Mater.*, 2022, **10**, 2200228.

16 Y. Song, H. Yu, B. Li, X. Li, Y. Zhou, Y. Li, C. He, G. Zhang, J. Luo and S. Zhao, A ferroelectric nonlinear optical crystal for deep-UV quasi-phase-matching, *Adv. Funct. Mater.*, 2024, **34**, 2310407.

17 L. Croitor, E. B. Coropceanu, A. V. Siminel, V. C. Kravtsov and M. S. Fonari, Polymeric Zn(II) and Cd(II) sulfates with bipyridine and dioxime ligands: Supramolecular isomerism, chirality, and luminescence, *Cryst. Growth Des.*, 2011, **11**, 3536–3544.

18 Y. Zhou, X. Zhang, Z. Xiong, X. Long, Y. Li, Y. Chen, X. Chen, S. Zhao, Z. Lin and J. Luo, Non-π-conjugated deep-ultraviolet nonlinear optical crystal $K_2Zn_3(SO_4)(HSO_4)_2F_4$, *J. Phys. Chem. Lett.*, 2021, **12**, 8280–8284.

19 C.-L. Hu and J.-G. Mao, Recent advances on second-order NLO materials based on metal iodates, *Coord. Chem. Rev.*, 2015, **288**, 1–17.

20 Y. Suffren and I. Gautier-Luneau, Titanyl iodate-a promising material for infrared nonlinear optics showing structural similarities with KTP, *Eur. J. Inorg. Chem.*, 2012, **2012**, 4264–4267.

21 K. Kato, Second–harmonic generation at 2660 Å in $BeSO_4·4H_2O$, *Appl. Phys. Lett.*, 1978, **33**, 413–414.

22 Y. Lu, X. Jiang, C. Wu, L. Lin, Z. Huang, Z. Lin, M. G. Humphrey and C. Zhang, Molecular engineering toward an enlarged optical band gap in a bismuth sulfate via homovalent cation substitution, *Inorg. Chem.*, 2021, **60**, 5851–5859.

23 Y. Sun, C. Lin, H. Tian, Y. Zhou, J. Chen, S. Yang, N. Ye and M. Luo, $A_2BeS_2O_8$ (A = NH_4, K, Rb, Cs) deep ultraviolet nonlinear optical crystals, *Chem. Mater.*, 2022, **34**, 3781–3788.

24 Y. Shen, X. Xue, W. Tu, Z. Liu, R. Yan, H. Zhang and J. Jia, Synthesis, crystal structure, and characterization of a noncentrosymmetric sulfate $Cs_2Ca_2(SO_4)_3$, *Eur. J. Inorg. Chem.*, 2020, 854–858.

25 X. Dong, L. Huang, C. Hu, H. Zeng, Z. Lin, X. Wang, K. M. Ok and G. Zou, $CsSbF_2SO_4$: An excellent ultraviolet nonlinear optical sulfate with a $KTiOPO_4$ (KTP)-type structure, *Angew. Chem., Int. Ed.*, 2019, **58**, 6528–6534.

26 C. Wu, X. Jiang, Y. Hu, C. Jiang, T. Wu, Z. Lin, Z. Huang, M. G. Humphrey and C. Zhang, A lanthanum ammonium sulfate double salt with a strong SHG response and wide deep-UV transparency, *Angew. Chem., Int. Ed.*, 2022, **61**, e202115855.

27 Y.-L. Li, M.-Y. Ji, C.-L. Hu, J. Chen, B.-X. Li, Y. Lin and J.-G. Mao, Explorations of new SHG materials in mercury

Iodate sulfate system, *Chem. – Eur. J.*, 2022, **28**, e202200001.

28 Q. Xu, X. Jiang, C. Wu, L. Lin, Z. Huang, Z. Lin, M. G. Humphrey and C. Zhang, $Rb_3In(SO_4)_3$: A defluorinated mixed main-group metal sulfate for ultraviolet transparent nonlinear optical materials with a large optical band gap, *J. Mater. Chem. C.*, 2021, **9**, 5124–5131.

29 Q. Wei, C. He, K. Wang, X.-F. Duan, X.-T. An, J.-H. Li and G.-M. Wang, $Sb_6O_7(SO_4)_2$: A promising ultraviolet nonlinear optical material with an enhanced second-harmonic-generation response activated by SbIII lone-pair stereoactivity, *Chem. – Eur. J.*, 2021, **27**, 5880–5884.

30 F. Yang, L. Wang, Y. Ge, L. Huang, D.-J. Gao, J. Bi and G. Zou, $K_4Sb(SO_4)_3Cl$: The first apatite-type sulfate ultraviolet nonlinear optical material with sharply enlarged birefringence, *J. Alloys Compd.*, 2020, **834**, 155154.

31 Z.-H. Yue, Z.-T. Lu, H.-G. Xue and S.-P. Guo, $KBiCl_2SO_4$: The first bismuth chloride sulfate being second-order nonlinear optical active, *Cryst. Growth Des.*, 2019, **19**, 3843–3850.

32 H.-X. Tang, Y.-X. Zhang, C. Zhuo, R.-B. Fu, H. Lin, Z.-J. Ma and X.-T. Wu, A niobium oxyiodate sulfate with a strong second-harmonic-generation response built by rational multi-component design, *Angew. Chem., Int. Ed.*, 2019, **58**, 3824–3828.

33 X. Dong, L. Huang, H. Zeng, Z. Lin, K. M. Ok and G. Zou, High-performance sulfate optical materials exhibiting giant second harmonic generation and large birefringence, *Angew. Chem., Int. Ed.*, 2022, **61**, e202116790.

34 C. Wu, T. Wu, X. Jiang, Z. Wang, H. Sha, L. Lin, Z. Lin, Z. Huang, X. Long, M. G. Humphrey and C. Zhang, Large second-harmonic response and giant birefringence of $CeF_2(SO_4)$ induced by highly polarizable polyhedra, *J. Am. Chem. Soc.*, 2021, **143**, 4138–4142.

35 T. Wu, X. Jiang, Y. Zhang, Z. Wang, H. Sha, C. Wu, Z. Lin, Z. Huang, X. Long, M. G. Humphrey and C. Zhang, From $CeF_2(SO_4)·H_2O$ to $Ce(IO_3)_2(SO_4)$: Defluorinated homovalent substitution for strong second-harmonic-generation effect and sufficient birefringence, *Chem. Mater.*, 2021, **33**, 9317–9325.

36 Z. Guo, J. Li, J. Liang, C. Wang, X. Zhu and T. He, Regulating optical activity and anisotropic second-harmonic generation in zero-dimensional hybrid copper, *Nano Lett.*, 2022, **22**, 846–852.

37 C. Yuan, X. Li, S. Semin, Y. Fen, T. Rasing and J. Xu, Chiral lead halide perovskite nanowires for second-order nonlinear optics, *Nano Lett.*, 2018, **18**, 5411–5417.

38 J. Lin, M.-H. Lee, Z.-P. Liu, C. Chen and C. J. Pickard, Mechanism for linear and nonlinear optical effects in β-BaB_2O_4 crystals, *Phys. Rev. B: Condens. Matter Mater. Phys.*, 1999, **60**, 13380–13389.

39 X.-M. Li, J. Liu, C. Zhao, J.-L. Zhou, L. Zhao, S.-L. Li and Y.-Q. Lan, Strategic hierarchical improvement of superprotonic conductivity in a stable metal-organic framework system, *J. Mater. Chem. A*, 2019, **7**, 25165–25171.

40 W.-L. Xie, X.-M. Li, J.-M. Lin, L.-Z. Dong, Y. Chen, N. Li, J.-W. Shi, J.-J. Liu, J. Liu, S.-L. Li and Y.-Q. Lan, Keeping

7032 | *Inorg. Chem. Front.*, 2024, **11**, 7026–7033

This journal is © the Partner Organisations 2024

superprotonic conductivity over a wide temperature region via sulfate hopping sites-decorated zirconium-oxo clusters, *Small*, 2022, **18**, 2205444.

41 B. L. Chaloux, J. A. Ridenour, M. D. Johannes and A. Epshteyn, Comparing proton conduction in potassium and ammonium borosulfate-isostructural inorganic polyelectrolytes exhibiting high proton mobility, *Adv. Energy Sustainability Res.*, 2022, **3**, 2200029.

42 J. M. Polfus, T. Norby and R. Bredesen, Protons in oxysulfides, oxysulfates, and sulfides: A first-principles study of La_2O_2S, $La_2O_2SO_4$, $SrZrS_3$, and $BaZrS_3$, *J. Phys. Chem. C*, 2015, **119**, 23875–23882.

43 M. Zdanowska-Frączek, A. Gągor, K. Hołderna-Natkaniec, Cz. Pawlaczyk, Z. Czapla and P. Ławniczak, Structure, proton conductivity and molecular dynamics of guanidine zinc sulfate, *Solid State Ionics*, 2017, **303**, 113–118.

This journal is © the Partner Organisations 2024

Inorg. Chem. Front., 2024, **11**, 7026–7033 | **7033**